# Parameters of Gas Dissolution in Liquids Obtained by Isothermal Pressure Decay

**Maurice L. Rasmussen**
School of Aerospace and Mechanical Engineering, The University of Oklahoma, Norman, OK 73019

**Faruk Civan**
Mewbourne School of Petroleum and Geological Engineering, The University of Oklahoma, Norman, OK 73019

*DOI 10.1002/aic.11669*
*Published online November 10, 2008 in Wiley InterScience (www.interscience.wiley.com).*

*A rapid and effective data analysis and interpretation approach is developed and validated for simultaneous determination of the film-mass-transfer and diffusion coefficients from time-limited experimental data obtained by dissolving gas in liquids by the pressure-decay method under isothermal conditions. Whereas previous approaches require experimental data until equilibrium and only determine the diffusion coefficient, accurate and rapid estimation of both parameters are achieved using a shorter set of time-limited data, thereby reducing the errors owing to swelling by significant gas dissolution at later times. The equilibrium conditions can be predicted theoretically stemming from an analysis of the time-limited data. This provides the estimates of the equilibrium pressure and gas solubility. This methodology not only yields accurate parameter values, but also alleviates the sufficiently large-time collection of pressure-decay data needed to essentially achieve equilibrium.* © 2008 American Institute of Chemical Engineers *AIChE J,* 55: 9–23, 2009
*Keywords: gas, liquid, film-mass-transfer, diffusion, coefficient, equilibrium pressure, solubility, pressure-decay, time-limited data*

## Introduction

Frequently, the values of the gas film-mass-transfer and diffusion coefficients and the equilibrium pressure and solubility are required for designing of the chemical processes involving the contact of various gases with liquids. Therefore, accurate determination of these parameters by suitable and practical experimental procedures is of continuing interest. The outstanding approaches to experimental measurements of the gas-diffusion coefficient and/or other relevant parameters, such as the interface-mass-transfer coefficient and the liquid swelling coefficient include the pressure decay (PD) method,[1–16] the constant pressure dissolving gas volumes (CPDGV) method,[17,18] the low-field nuclear magnetic resonance (NMR) spectra change method,[19,20] the X-ray computer-assisted tomography (CAT) method,[20] the gas permeation through an immobilized liquid membrane (ILM) method implemented in a diffusion cell,[21] and the dynamic pendant drop volume analysis (DPDVA) method.[22]

Among the various approaches to experimental determination of these parameters the pressure decay (PD) method has been the preferred approach because of its convenience, simplicity, and accuracy. In this method, the decline of the gas pressure with time is measured after certain amounts of gas and liquid are brought into contact instantaneously in a conventional pressure-volume-temperature (PVT)-cell (see Figure 1). The NMR and CAT methods are nondestructive methods, based on the determination of the average concentrations of a solute (a gas or a solvent), dissolved in a liquid contained in a PVT-cell at various times. The ILM method utilizes the measurement of the flux of gases through an immobilized liquid membrane by the pressure rise in the permea-

Correspondence concerning this article should be addressed to F. Civan at fcivan@ou.ed.

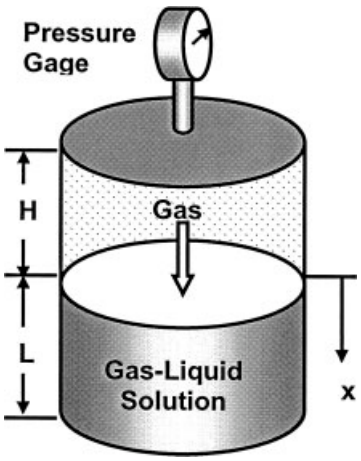


**Figure 1. Schematic PVT-cell used for measurement of gas diffusivity in liquids.**

meter chamber. The DPDVA method is based on the measurement of the pendant drop shape at various times during a solute dissolution into the liquid drop. Then, appropriate phenomenological mathematical models are facilitated for parameter estimation by fitting of the model results to experimental data.

The sensitivity of the results obtained by the PD, NMR, and CAT methods with respect to the sample size is low, because of the relatively large liquid volumes used in the PVT-cells. The sensitivity of the results obtained by the DPDVA method with respect to the sample size is very high, because of the significantly small liquid volume contained in a pendant drop. Therefore, the effect of swelling is amplified in the DPDVA method particularly allowing also for determination of the liquid swelling coefficient. However, the parameter estimation quality is prone to errors because of the loss of accuracy owing to high-sensitivity to volume of small drops, and the requirement of the considerations for the rapidly attained nonideal solution conditions in the analytical interpretation methods. These errors can be conveniently avoided in the PVT measurements if an early data analysis interpretation method is used, as described in this study, so that the dissolved gas concentration is still sufficiently low to justify the ideal solution behavior and negligible swelling effects assumptions. The sensitivity of the results obtained by the ILM method is in between because the amount of liquid that a porous membrane can hold is much larger than the pendant drop-size, and much smaller than the liquid capacity of a PVT-cell.

There are several motivations for this study dealing with an improvement on the analysis and interpretation of the data obtained by the pressure decline method. First, although this experimental procedure is straightforward and practical, the accuracy of the late pressure data collected is prone to errors owing to high-pressure gas leaks when experiments have to be run over sufficiently long periods of time, usually in the order of two months, in order to apply data interpretation methods requiring the measurement of the gas pressure at equilibrium. Further, the accuracy of the estimated parameter values may be subjected to the effect of higher concentrations of the dissolved gas in the liquid phase, because the available interpretation methods consider dilute solutions, and, therefore, neglect the effects of the liquid swelling and gas concentration on the diffusion coefficient. Second, the majority of the previous analytical data interpretation methods[4,5,6,7,19,20,21] involve the application of rather simplified models for estimation of the gas diffusion coefficient. The interpretation method presented by Yang and Gu[22] is a very tedious finite-element numerical solution approach, which is subject to significant errors owing to the sensitivity of the results to the small pendant drop-size and rapidly attained nonideal solution behavior. Third, most methods determine the gas diffusion coefficient and ignore the determination of the film-mass-transfer coefficient. A discussion of relevant issues can be found in Tharanivasan et al.[9] and Civan and Rasmussen.[13–16]

The choice of the gas/liquid interface boundary condition for the diffusing gas component has varied with the different researchers and affected the quality of the resulting data interpretation methods. Tharanivasan et al.[9] emphasized that the proper choice of the boundary and gas/liquid interface conditions can be instrumental in accurately determining the parameters of gas diffusion in liquids. Sheikha et al.[10–12] and Jamialahmadi et al.[18] considered a thermodynamic equilibrium at the interface between the gas and liquid phases. Consequently, applying the film theory, the equilibrium dissolved gas concentration in the liquid phase near the interface corresponding to the gas pressure in the gas phase was considered as the boundary condition. Jamialahmadi et al.[18] measured their experimental data while maintaining the applied gas pressure constant above the liquid phase. Hence, their interface boundary condition is simple; dictating that the dissolved gas concentration near the interface remains constant at the saturation value. However, Sheikha et al.[10–12] expressed this relationship according to the Henry's law in interpretation of the pressure decay data, the application of which is limited to ideal dilute solution conditions. Further, the interface boundary condition derived by Sheikha et al.[10–12] by combining the gas phase mass balance with the Henry's law neglects the variation of the volume of the gas phase by swelling of the liquid phase owing to gas dissolution, and the term involving the partial derivative of the real gas deviation factor with respect to pressure (See Appendix A). Nevertheless, the swelling effect may be neglected for their experimental conditions, but the variation of the real gas deviation factor may not be negligible. The nonequilibrium boundary condition used by Civan and Rasmussen,[16] frequently referred to as the Robin condition, may conveniently alleviate the difficulties associated with the aforementioned interface boundary conditions because it is generally applicable regardless of the varying conditions of the interface.

This article presents a convenient modification to the data interpretation method proposed by Civan and Rasmussen[13–16] so that it can be applied for rapid and accurate determination of the gas diffusion and film-mass-transfer coefficients using only the time-limited data, independent of any *a priori* estimate of the equilibrium conditions. This eliminates the effect of the inaccuracies of the late-time data due to possible gas leaks and liquid swelling during the laboratory tests conducted until equilibrium is approached. The validity of the new method is demonstrated by comparing the new parameter values with those obtained with the previous methods. In addition, a new analytical procedure is provided to obtain the

estimates of the equilibrium pressure and gas solubility without needing to run tests until equilibrium.

## Formulation for Analysis of Pressure Decay Tests

Figure 1 depicts the schematic PVT cell used for the isothermal pressure-decline method. The mass lost in a gaseous region in an isothermal quasi-equilibrium pressure-decay process is equal to the mass gained in an adjacent liquid region undergoing a quasi-equilibrium isothermal diffusion process. The mass is transferred across a gas-liquid interface surface. It is assumed that the total amount of gas lost or gained in these processes is small compared to the amount of liquid that absorbs it, and thus that the change in volume in each of the two regions is negligible (See Appendix A).

### *Gas Dissolution in the liquid phase*

We model the liquid region as a cylinder having a cross-section area $A$, and length $L$, and $x$ and $t$ represent the distance from the original gas-liquid interface and the time. Let $c_o$, $c$, and $c^*$ denote the initial, instantaneous, and equilibrium mass densities for the gas in the liquid-gas mixture (solution) region, and let $D$ represent the gas-liquid diffusion coefficient (taken as a constant). Then the dimensionless gas concentration, distance, and time are defined as

$$c_D = \frac{c - c_o}{c^* - c_o} \tag{1}$$

$$x_D = \frac{x}{L} \tag{2}$$

$$t_D = \frac{Dt}{L^2} \tag{3}$$

The gas concentration is governed by the classical diffusion equation

$$\frac{\partial c_D}{\partial t_D} = \frac{\partial^2 c_D}{\partial {x_D}^2}, \quad 0 \le x_D \le 1,\ t_D > 0 \tag{4}$$

with the initial condition

$$c_D = 0, \quad 0 \le x_D \le 1,\ t_D = 0 \tag{5}$$

and the boundary conditions

$$-\frac{\partial c_D}{\partial x_D} = k_D(1 - c_D), \quad x_D = 0, \quad t_D > 0 \tag{6}$$

$$\frac{\partial c_D}{\partial x_D} = 0, \quad x_D = 1,\ t_D > 0 \tag{7}$$

The parameter $k_D$ is the mass-transfer Biot number, given by

$$k_D \equiv kL/D \tag{8}$$

where $k$ is the interface film mass-transfer coefficient that is a model parameter.

The total mass of gas transferred to the liquid region by diffusion at any instant of time is given by

$$\Delta m = AL \int_0^1 (c - c_o) dx_D = AL(c^* - c_o) Q_D(t_D) \tag{9}$$

where $Q_D(t_D)$ is the nondimensional mass-accumulation function, which is also equal to the volumetric average of $c_D(x_D,t_D)$ in the liquid phase, given by

$$Q_D(t_D) \equiv \int_0^1 c_D(x_D, t_D) dx_D \tag{10}$$

### *Pressure decline in the gas phase*

Now consider the changes that occur in the gaseous region of a PVT-cell due to a change in pressure under isothermal conditions. The relation between the pressure $p$, volume $V$, mass $m$, and temperature $T$ of a gas in state of equilibrium is given by the thermal equation of state

$$pV = m\left(\frac{\Re}{M}\right) TZ(p,T) \tag{11}$$

where $\Re$ is the universal gas constant, $M$ is the molecular weight of the gas, and $Z(p,T)$ is an empirical function of pressure and temperature called the real-gas deviation factor. The initial volume of the gaseous region is

$$V_o = AH \tag{12}$$

where $A$ is the cross-sectional area of the PVT-cell, and $H$ is the thickness of the gas region.

We now suppose that the changes in the gaseous region are constrained by the diffusion processes across the gas-liquid interface to be so slow and weak that the state of the gas during the change does not differ from local equilibrium. For such a quasi-equilibrium and isothermal process, the decrease in the amount of mass in the region is determined by simply the decrease from an initial pressure $p_o$ to an instantaneous pressure $p$, consistent with Eq. 11 and assuming negligible volume changes

$$\Delta m = \frac{MV_o}{\Re T}\left[\frac{p_o}{Z_o} - \frac{p}{Z}\right] = m_o \frac{\left[\frac{p_o}{Z_o} - \frac{p}{Z}\right]}{\frac{p_o}{Z_o}} \tag{13}$$

where $Z_o \equiv Z(p_o,T)$, and $m_o$ is the initial amount of the gas. Setting the mass lost by the gaseous region (Eq. 13) equal to the mass gained by the liquid region (Eq. 9) yields

$$Q_D(t_D) = \frac{MH}{\Re TL(c^* - c_o)}\left[\frac{p_o}{Z_o} - \frac{p(t)}{Z}\right] \tag{14}$$

This is the fundamental equation pertaining to the pressure-decay method of data analysis. A useful alternative form can be found by noting that equilibrium obtains as $t_D \to \infty$ in which case $Q_D \to 1$, and $p \to p^*$, and Eq. 14 takes the form

$$1 = \frac{MH}{\Re TL(c^* - c_o)}\left[\frac{p_o}{Z_o} - \frac{p^*}{Z^*}\right] \tag{15}$$

This is essentially a relation between the equilibrium pressure and the equilibrium concentration. Dividing Eq. 14 by Eq. 15 gives

$$Q_D(t_D) = \frac{\frac{p_o}{Z_o} - \frac{p(t)}{Z}}{\frac{p_o}{Z_o} - \frac{p^*}{Z^*}} \tag{16}$$

Suppose that the pressure ratio on the right side of Eq. 16 is a measured function of time, and that the mass-accumulation $Q_D(t_D)$ is a known function of time stemming from a solution of the theoretical diffusion problem with arbitrary diffusion coefficient $D$, and interface mass-transfer coefficient $k$. Then $D$ and $k$ can be determined by a suitable fitting of the theoretical curves with the experimental data subject to Eq. 16, with the physical time taken as the common factor. The trouble with this scenario is that generally the equilibrium pressure $p^*$ has not been adequately determined. Strictly, $p^*$ is the value of the pressure as $t_D \to \infty$. Thus, for real sets of data taken over finite periods of time, $p^*$ must be found by some extrapolation method or another. Because of this difficulty, as well as others associated with very long acquisition times, we consider an alternative approach.

Let us select a late-time data point, supported by a large confidence level, say $p = p_R$ at $t = t_R$, to be used as a reference point. Let all the data that occur before or equal to the time $t_R$ be referred to as the time-limited set of data. At the reference point we have, from Eq. 16

$$Q_D(t_{DR}) = \frac{\frac{p_o}{Z_o} - \frac{p_R}{Z_R}}{\frac{p_o}{Z_o} - \frac{p^*}{Z^*}} \tag{17}$$

Now all the time-limited data can be renormalized by dividing Eq. 16 by Eq. 17

$$Q_R(t_D; t_{DR}) \equiv \frac{Q_D(t_D)}{Q_D(t_{DR})} = \frac{\frac{p_o}{Z_o} - \frac{p(t)}{Z}}{\frac{p_o}{Z_o} - \frac{p_R}{Z_R}} \tag{18}$$

The best estimate values of the diffusion coefficient $D$, and the film mass-transfer coefficient $k$, are, thus, determined by substituting the analytical solution of Eqs. 4–7 for $Q_D(t_D)$ and $Q_D(t_{D_k})$, and the experimentally measured pressure values at various times, as described in subsequent sections.

### *Basic solutions for the diffusion problem*

An exact solution of Eqs. 4–7 for $c_D$ obtained by a Fourier-series analysis when the length $L$ is finite was given by Walas.[23] When this solution is substituted into Eq. 10 for $Q_D$, and the integration carried out, the result is

$$Q_D(t_D) = 1 - 4\sum_{m=1}^{\infty} \frac{\sin^2\lambda_m}{\lambda_m[2\lambda_m + \sin(2\lambda_m)]} e^{-\lambda_m^2 t_D} \tag{19}$$

where $\lambda_m$ denotes the roots of the eigenvalue equation

$$\lambda \tan\lambda = k_D(\lambda) \tag{20}$$

The complete infinite-series satisfies the relation $Q_D(0) = 0$.

When the nondimensional time $t_D$ is sufficiently large, only the first term in the Fourier series is important, and the corresponding result is called the long-time approximation

$$Q_D^{LT}(t_D; \lambda) = 1 - Q_1(\lambda) e^{-\lambda^2 t_D} \tag{21}$$

where

$$Q_1(\lambda) \equiv \frac{4\sin^2\lambda}{\lambda[2\lambda + \sin(2\lambda)]} \tag{22}$$

The parameter is the lowest positive root ($0 \le \lambda \le \pi/2$) of Eq. 20. It is interesting and useful to note that taking the natural logarithm of Eq. 21 leads to the result

$$\ln(1 - Q_D^{LT}(t_D, \lambda)) = \ln(Q_1(\lambda)) - \lambda^2 t_D \tag{23}$$

Thus, plotting the natural logarithm of $(1 - Q_D^{LT}(t_D;\lambda))$ against $t_D$ produces a straight-line with both the y-axis intercept, and the slope of the line determined by the value of $\lambda$.

The short-time approximation is obtained by applying the semi-infinite ($L \to \infty$) solution given by Crank[24] to Eq. 10 as follows

$$Q_D^{ST}(t_D; \lambda) = \frac{1}{k_D}\left[\exp(k_D^2 t_D)\mathrm{erfc}(k_D\sqrt{t_D}) - 1 + 2k_D\sqrt{\frac{t_D}{\pi}}\right] \tag{24}$$

where $k_D(\lambda)$. is given by the same eigenvalue equation (Eq. 20) as before. Note when the mass-transfer Biot number is very large $k_D \to \infty$, corresponding to $\lambda$ going to its upper limit $\lambda \to \pi/2$, and with $t_D$ held fixed, that Eq. 24 reduces to

$$Q_D^{ST}\left(t_D; \frac{\pi}{2}\right) = 2\sqrt{\frac{t_D}{\pi}} \tag{25}$$

This is the result that would have been obtained if the Dirichlet condition $c_D = 1$ had been imposed as the interface boundary condition at $x_D = 0$. On the other hand, when $k_D$ is held fixed, the short-time solution, Eq. 24, itself has two time ranges embedded within it that are of interest. For very small times, Eq. 24 can be expanded for small $z = k_D\sqrt{t_D}$ to obtain

$$Q_D^{ST}(t_D) \cong \frac{1}{k_D}\left[z^2 - \frac{4}{3\sqrt{\pi}}z^3 + \frac{z^4}{2} - \frac{8}{15\sqrt{\pi}}z^5 + \frac{z^6}{6} - \frac{16}{105\sqrt{\pi}}z^7 + \ldots\right], \quad z \to 0 \tag{26}$$

Thus, for finite $k_D$, when $Q_D$ is plotted against $\sqrt{t_D}$, the initial slope is always zero.

When $t_D$ is allowed to become large, that is $t_D \to \infty$, then Eq. 24 for the short-time behavior approaches the asymptote

$$Q_{Da}^{ST}(t_D; \lambda) = 2\sqrt{\frac{t_D}{\pi}} - \frac{1}{k_D}\ , \ \sqrt{t_D} \to \infty \tag{27}$$

In practice, the large-time behavior of the short-time approximation applies to some mid-range of the overall time variation. Thus, when $Q_D$ is plotted against $\sqrt{t_D}$, we might expect some mid-range portion of the curve to be nearly parallel to, or almost coincident with, the straight-line asymptote given by Eq. 27.

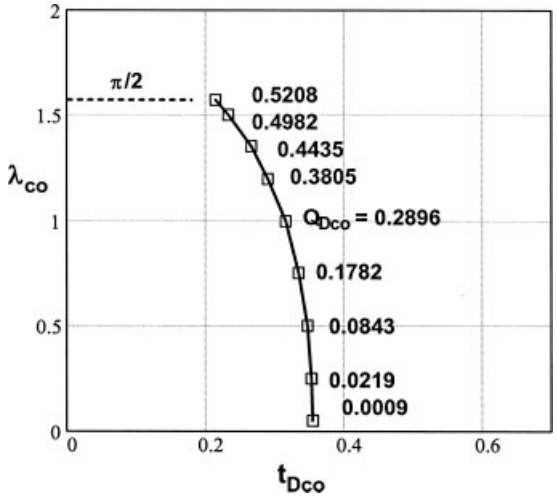


**Figure 2. Coordinates for the crossover point for the long-time and short-time approximations.**

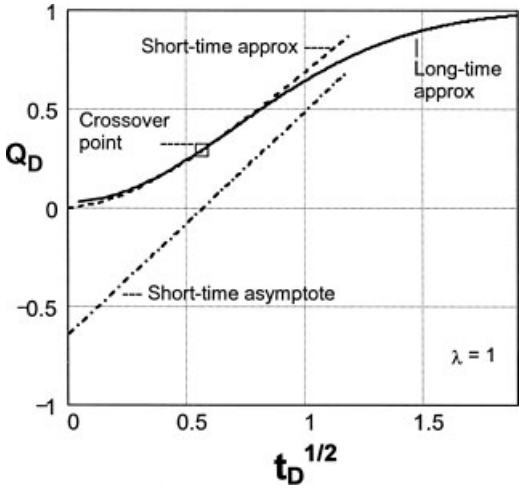


**Figure 4. Example showing long-time and short-time approximations for $Q_D$ vs. $\sqrt{t_D}$ and $\lambda = 1$.**

## Data Interpretation and Parameter Estimation Procedure

The objective of this article is to interpret experimental data and infer from it the values of the diffusion coefficient $D$, and the interface mass-transfer coefficient $k$. When a given set of data is plotted on one coordinate vs. another, the nature of the coordinates can make a difference on the insight that the plot provides. To accomplish this objective, we wish to use the short-time approximation by Eq. 24 together with the long-time approximations, either in the form of Eq. 21, or in its counterpart logarithmic form of Eq. 23, to analyze data generated over the whole time range in the form of $Q_D$ vs. time $t$ stemming from the pressure decline relation Eq. 16. The coordinates of the crossover (CO) points, that is, the intersection of the short- and long-time curves, are shown in Figure 2. The reason this is possible is that, whereas the short-time approximation is basically valid for short times, but fails for very large times, and because the long-time approximation is basically valid for long times, but fails for very small times, they share a common intermediate-time overlap region in which they are both valid (Civan and Rasmussen[13–16]) (See Figures 3 through 5). In $Q_D$ vs. $\sqrt{t_D}$ plots, this overlap region is asymptotic to, and nearly coincides with, the straight-line given by Eq. 27 for values of $\lambda \geq 1.35$, as exemplified by Figure 3. For, $\lambda < 1.35$, however, the asymptote is approached too slowly to adequately represent the overlap region, as shown in Figure 4 for $\lambda = 1$. Plots of $Q_D$ vs. $\sqrt{t_D}$, emphasize the short time. On the other hand, plots of $\ln(1 - Q_D)$ vs. $t_D$ or $\log(1 - Q_D)$ vs. $t_D$ emphasize the long time (Figure 5). The long-time approximation Eq. 23 is characterized by a straight line on the semi-log plots. Note that $Q_D$ varies between zero and unity as $t_D$ goes from zero to infinity.

It is important to note that the experimental data are plotted as a function of the real time $t$, and not the nondimensional time $t_D$. Thus, in the theoretical formulas we must make the substitution

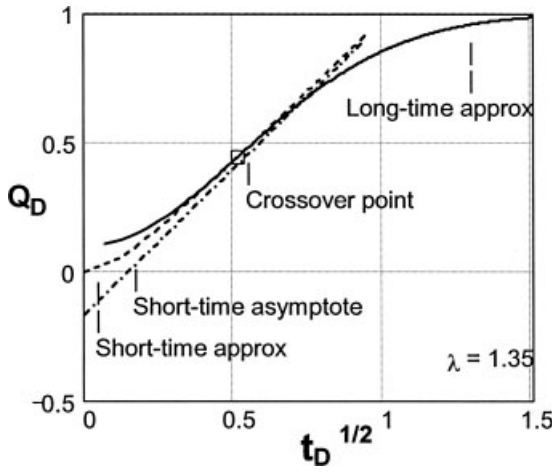


**Figure 3. Example showing long-time and short-time approximations for $Q_D$ vs. $\sqrt{t_D}$ and $\lambda = 1.35$.**

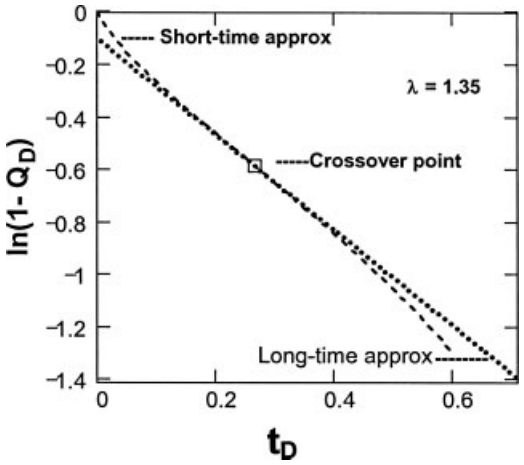


**Figure 5. Example showing long-time and short-time approximations on semi-log plot $\ln(1 - Q_D)$ vs $t_D$ for $\lambda = 1.35$.**

$$t_D = \frac{t}{t_C} \tag{28}$$

where the coefficient $t_C$ is a characteristic time, and is given by

$$t_c = \frac{L^2}{D} \tag{29}$$

Thus, the theoretical formulas cannot be plotted against the experimental data unless $t_C$ is specified arbitrarily or developed by some systematic means. In this regard, it is appropriate to express the short-time and long-time approximations Eqs. 24, 21, and 23 functionally as

$$Q_D^{ST}(t; t_C, \lambda) = Q_D^{ST}\left(\frac{t}{t_C}; \lambda\right) \tag{30}$$

$$Q_D^{LT}(t; t_C, \lambda) = Q_D^{LT}\left(\frac{t}{t_C}; \lambda\right) \tag{31}$$

$$L^{ST}(t; t_C, \lambda) \equiv \ln\left(1 - Q_D^{ST}\right) \tag{32}$$

$$L^{LT}(t; t_C, \lambda) \equiv \ln(1 - Q_D^{LT}) = \ln[Q_1(\lambda)] - \frac{\lambda^2}{t_C} t \tag{33}$$

For the purposes of data analysis, these functions now depend on the physical time $t$ and two parameters $t_C$ and $\lambda$.

### *Determination of $t_C$ and $\lambda$ for a given set of data and given equilibrium pressure*

Now suppose that the data are given at $n$ discrete points designated by $i$ going from 0 to $(n - 1)$, with $i = 0$ representing the first nonzero time point. After plotting the data vs. $\sqrt{t}$ and on the semilog plots, that is, $Q_{Di}$ vs. $\sqrt{t_i}$ and $L_i \equiv \ln(1 - Q_{D_i})$ vs. $t_i$, pick a point $i_m$ that separates the short-time data from the long-time data (a point near the crossover (CO) point or the intersection of the short- and long-time curves, say), and form the following squared-error functions

$$E^{ST}(t_C, \lambda; i_m) = \sum_{i=0}^{i_m} \left(Q_{D_i} - Q_D^{ST}\left(\frac{t_i}{t_C}, \lambda\right)\right)^2 \tag{34}$$

$$E^{LT}(t_C, \lambda; i_m) = \sum_{i=i_m}^{n-1} \left(Q_{D_i} - Q_D^{LT}\left(\frac{t_i}{t_C}, \lambda\right)\right)^2 \tag{35}$$

$$E(t_C, \lambda; i_m) = E^{ST}(t_C, \lambda; i_m) + E^{LT}(t_C, \lambda; i_m) \tag{36}$$

Equation 34 represents the total squared error between the short-time data points and the short-time function (Eq. 24) for arbitrary values of $t_C$ and $\lambda$, and Eq. 35 represents the corresponding total squared error between the long-time data points and the long-time function (Eq. 21). Equation 36 represents the total squared error over the whole range of data plotted as $Q_D$ vs. $\sqrt{t}$ for arbitrary values of $t_C$ and $\lambda$. For the semilog plots, we have correspondingly

$$E_L^{ST}(t_C, \lambda; i_m) = \sum_{i=0}^{i_m} \left(L_i - L^{ST}\left(\frac{t_i}{t_C}, \lambda\right)\right)^2 \tag{37}$$

$$E_L^{LT}(t_C, \lambda; i_m) = \sum_{i=i_m}^{n-1} \left(L_i - L^{LT}(\frac{t_i}{t_C}, \lambda)\right)^2 \tag{38}$$

$$E_L(t_C, \lambda; i_m) = E_L^{ST}(t_C, \lambda; i_m) + E_L^{LT}(t_C, \lambda; i_m) \tag{39}$$

The best-estimate values for the two parameters $t_C$ and $\lambda$ for a given set of data are determined by the least-squares regression of the theoretical curves to the data (See Chapra and Canale[25]) to minimize the function $E(t_C,\lambda;i_m)$ defined by Eq. 36 for the $Q_D$ vs.$\sqrt{t}$ plots, or for the function $E_L(t_C,\lambda;i_m)$ defined by Eq. 39, representing the semilog plots.

Note that the natural logarithm of the long-time approximation as it appears in Eq. 33 leads to a straight line when the natural logarithm $\ln(1 - Q_D^{LT})$ is identified with the $y$-axis, and the time $t$ is identified with the $x$-axis

$$\ln(1 - Q_D^{LT}) = -a_{LT} - b_{LT} t \tag{40}$$

where the coefficients $-a_{LT}$ and $-b_{LT}$ are the values of the $y$-axis intercept, and the slope that render the total squared error $E_L^{LT}$ (Eq. 38) a minimum. The negative signs are inserted in anticipation that the intercept, and the slope will always be negative (See Figure 5). A comparison of this result with Eq. 33 leads to the following identification

$$a_{LT} = -\ln[Q_1(\lambda)] \tag{41}$$

$$b_{LT} = \frac{\lambda^2}{t_C} \tag{42}$$

Thus, the parameter $\lambda$ is determined implicitly entirely in terms of the value of the $y$-axis intercept, which enables the mass-transfer Biot number $k_D$ to be determined from Eq. 20. Equation 42 shows that the characteristic time $t_C$ is inversely proportional to the slope and is determined by

$$t_C = \frac{\lambda^2}{b_{LT}} \tag{43}$$

This in turn allows the diffusion coefficient to be determined by means of Eq. 29

$$D = \frac{L^2}{t_C} = \frac{L^2}{\lambda^2} b_{LT} \tag{44}$$

The diffusion coefficient is inversely proportional to the characteristic time and proportional to the slope of the line. Finally, the interface mass-transfer coefficient $k$ is determined by Eq. 8 as

$$k = \frac{D}{L} k_D \tag{45}$$

If the value of the equilibrium pressure $p^*$ appearing in Eq.16, which is the fundamental basis for the forgoing analysis, was obtained very accurately, and if there were no experimental error in the data, and no scatter; in other words, if the data were perfect, then a regression analysis of the short-time data by means of Eq. 37 would yield essentially the same results. However, various factors (Civan and Rasmussen[16]) and the mixing induced by natural convection in both

the gas and liquid phases may introduce some errors. See Appendix B for estimation of error.

It is possible under restrictive conditions to obtain analytic results for the short-time data. When it is taken into account that Eq. 27 for the long-time asymptote for the short-time behavior gives a straight line when plotted against $\sqrt{t}$, then a regression analysis of the function

$$E_a^{ST}(t_C,\lambda;i_m)=\sum_{i=i_o}^{i_m}\left(Q_{D_i}-Q_{Da}^{ST}\left(\frac{t_i}{t_C},\lambda\right)\right)^2 \tag{46}$$

leads to a straight line of the form

$$Q_{Da}^{ST}=-a_{ST}+b_{ST}\sqrt{t} \tag{47}$$

where the intercept and the slope are identified as

$$a_{ST}=\frac{1}{k_D} \tag{48}$$

$$b_{ST}=\frac{2}{\sqrt{\pi t_C}} \tag{49}$$

It follows that

$$k_D=\frac{1}{a_{ST}} \tag{50}$$

$$t_C=\frac{4}{\pi b_{ST}^2} \tag{51}$$

Now $\lambda$ can be determined implicitly from Eq. 20, and the diffusion coefficient $D$ is determined again by means of Eq. 29

$$D=\frac{\pi L^2 {b_{ST}}^2}{4} \tag{52}$$

Finally, the interface mass-transfer coefficient $k$ can be calculated from Eq. 8 as

$$k=\frac{D}{L}k_D=\frac{D}{La_{ST}} \tag{53}$$

Using the aforementioned results for the short-time asymptote can produce reasonable approximations for $\lambda$ and $t_C$ only when the asymptote provides a reasonable approximation to the short-time approximation itself in the vicinity of the crossover (CO) point. This is arguably true for the case of $\lambda = 1.35$ shown in Figure 3, but not true for the case of $\lambda = 1$ shown in Figure 4. Notice also that some of the data points that lie close to the origin should be excluded from the summation indicated in Eq. 46, because in general the straight line does not pass though the origin. The symbol $i_o$ represents the first data point to be included. This correlation of the data represents the midrange straight-line character on a plot of $Q_D$ vs. $\sqrt{t}$, valid when $\lambda \geq 1.35$.

The values of $t_C$ and $\lambda$ so determined by the aforementioned methods depend on the choice of $i_m$, that is, how the data field was separated into parts that represent early-time and late-time behaviors. The squared-error functions $E_L^{LT}(t_C,\lambda;i_m)$ and $E_a^{ST}(t_C,\lambda;i_m)$ were minimized holding $i_m$ fixed. The whole procedure should be repeated for different values of $i_m$ until the least value of each of the squared-error functions is found, those providing the trio of values for $t_C$,$\lambda$, and $i_m$ sought after. The value of $i_m$ should correspond closely to the crossover point.

Apart from the subjective nature of obtaining a good value for the equilibrium pressure, by a manual extrapolation from the long-time data, say, the subjective nature and other difficulties associated with using only parts of the data field to obtain values of $\lambda$ and $t_C$ (and, thus, $D$ and $k$) that presumably hold for the whole data field shed doubt on results (Civan and Rasmussen[16]).

### *Determination of $t_C$ and $\lambda$ for a given set of data by means of a specified end-point*

Let us now return to Eq. 17 and assume that the chosen reference point $Q_D(t_{DR})$, where $t_{DR} \equiv t_R/t_C$, is located well within the long-time description zone, such that, $Q_D(t_{DR}) = Q_D^{LT}(t_{DR};\lambda)$, and, thus, that

$$Q_D(t_{DR};\lambda)=1-Q_1(\lambda)e^{-\lambda^2 t_{DR}} \tag{54}$$

Now Eq. 17 can be expressed as

$$1-Q_1(\lambda)e^{-\lambda^2 t_{DR}}=\frac{\frac{p_o}{Z_o}-\frac{p_R}{Z_R}}{\frac{p_o}{Z_o}-\frac{p^*}{Z^*}} \tag{55}$$

This equation allows the equilibrium pressure $p^*$ to be determined in terms of the reference pressure $p_R$, and the reference time $t_R$ after $\lambda$ and $t_C$ have been calculated by a suitable regression analysis. Then, the equilibrium solubility $c^*$ can be calculated by means of Eq. 15.

The time-limited diffusion function $Q_R(t_D)$, defined by Eq. 18, can now be expressed functionally as

$$Q_R(t_D;\lambda,t_{DR})\equiv\frac{Q_D(t_D)}{Q_D(t_{DR};\lambda)}=\frac{Q_D(t_D)}{1-Q_1(\lambda)e^{-\lambda^2 t_{DR}}} \tag{56}$$

The large-time approximation is

$$\begin{aligned}Q_R^{LT}(t_D;\lambda,t_{DR})&=\frac{Q_D^{LT}(t_D;\lambda)}{1-Q_1(\lambda)e^{-\lambda^2 t_{DR}}}=\frac{1-Q_1(\lambda)e^{-\lambda^2 t_D}}{1-Q_1(\lambda)e^{-\lambda^2 t_{DR}}}\\&=1-Q_1^*(\lambda,t_{DR})e^{-\lambda^2 t_D}\left(\frac{1-e^{-\lambda^2(t_{DR}-t_D)}}{1-e^{-\lambda^2 t_{DR}}}\right)\end{aligned} \tag{57}$$

where

$$Q_1^*(\lambda,t_{DR})\equiv\frac{Q_1(\lambda)(1-e^{-\lambda^2 t_{DR}})}{1-Q_1(\lambda)e^{-\lambda^2 t_{DR}}} \tag{58}$$

Notice that $Q_R^{LT}(t_D;\lambda,t_{DR}) \to 1$ as $t_D \to t_{DR}$ (or $t \to t_R$). Thus, this formulation is valid when $t \leq t_R$, or, in terms of the nondimensional variables, when $t_D \leq t_{DR}$, and, therefore, referred to as the time-limited formulation. When, $t_{DR} \to \infty$, then $Q_R^{LT}(t_D;\lambda,t_{DR}) \to Q_D^{LT}(t_D;\lambda)$, and the time-limited results reduce to the previous results where the equilibrium pressure was specified. The time-limited function $Q_R$ varies from zero

to unity as the time goes from zero to $t_R$. The natural logarithm rendition of Eq. 57 is

$$\ln(1-Q_R^{LT}(t_D;\lambda,t_{DR})) = \ln Q_1^*(\lambda,t_{DR}) - \lambda^2 t_D + \ln\left(\frac{1-e^{-\lambda^2(t_{DR}-t_D)}}{1-e^{-\lambda^2 t_{DR}}}\right) \quad (59)$$

An example of a semilog plot for this function is shown in Figure 6 for $\lambda = 1.50$ and $t_{DR} = 1$. In this case, Eq. 59 does not generate a straight line and is, in fact, singular at $t_D = t_{DR} = 1$. The last term in Eq. 59 describes the deviation from a straight line, and the first describes the $y$-axis intercept. Note that $Q_1^*(\lambda,t_{DR}) \leq Q_1(\lambda)$ because $Q_1 \leq 1$. The intercept is displaced downward slightly from the case where $t_{DR} \to \infty$.

It is interesting to note that the third term on the right side of Eq. 59 behaves as $-e^{-\lambda^2 t_{DR}}\lambda^2 t_D/(1-e^{-\lambda^2 t_{DR}})$ as $t_D \to 0$. Thus when $t_D$ is small, Eq. 59 behaves as the straight line

$$\ln(1-Q_R^{LT}(t_D;\lambda,t_{DR}))_a = \ln Q_1^*(\lambda,t_{DR}) - \frac{\lambda^2}{1-e^{-\lambda^2 t_{DR}}} t_D\ , \quad t_D \to 0 \quad (60)$$

This equation is the small-time asymptote for the large-time approximation, and is shown as the dashed line in Figure 6. Compare this result with the long-time approximation given by Eq. 23. When expressed as a function of the physical time, Eq. 60 takes the straight-line form

$$\ln(1-Q_R^{LT}(t_D;\lambda,t_{DR}))_a = -a_{LT}^R - b_{LT}^R t \quad (61)$$

where

$$a_{LT}^R \equiv -\ln Q_1^*(\lambda,t_{DR}) \quad (62)$$

and

$$b_{LT}^R \equiv \frac{\lambda^2}{t_C(1-e^{-\lambda^2 t_{DR}})} \quad (63)$$

are the $y$-axis intercept and the slope of the line. These expressions are the time-limited counterparts to Eqs. 40, 41, and 42. The slope of the straight line in the time-limited formulation, Eq. 63, is somewhat greater than the corresponding slope, Eq. 42.

The small-time behavior for the time-limited formulation is determined by

$$Q_R^{ST}(t_D;\lambda,t_{DR}) = \frac{Q_D^{ST}(t_D;\lambda)}{1-Q_1(\lambda)e^{-\lambda^2 t_{DR}}} \quad (64)$$

where the short-time function $Q_D^{ST}(t_D;\lambda)$ is given by Eq. 24. The straight-line asymptote for this relation is

$$Q_{Ra}^{ST} = -a_{ST}^R + b_{ST}^R\sqrt{t} \quad (65)$$

where the intercept and the slope are now

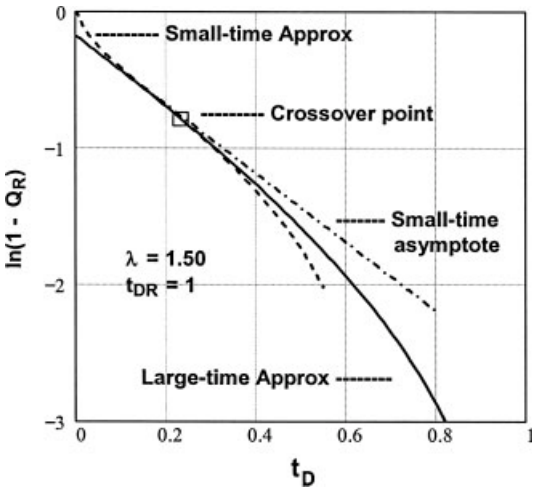


**Figure 6. Example showing time-limited large-time approximation on semi-log plot for $\lambda = 1.35$ and $t_{DR} = 2$.**

$$a_{ST}^R = \frac{1}{k_D\left[1-Q_1(\lambda)e^{-\lambda^2\frac{t_R}{t_C}}\right]} \quad (66)$$

$$b_{ST}^R = \frac{2}{\sqrt{\pi t_C}\left[1-Q_1(\lambda)e^{-\lambda^2\frac{t_R}{t_C}}\right]} \quad (67)$$

The ratio is given by

$$\frac{a_{ST}^R}{b_{ST}^R} = \frac{\sqrt{\pi t_C}}{2k_D} = \frac{\sqrt{\pi t_C}}{2\lambda\tan\lambda} \quad (68)$$

We can solve Eq. 68 for $t_C$, substitute back into Eq. 66, and obtain a single equation for $\lambda$.

The small-time and large-time approximations depend on the dimensionless time $t_D$, and the two parameters $\lambda$ and $t_{DR}$. From the point of view of data analysis, however, they depend on the real time $t$, and the three parameters $\lambda$, $t_C$ and $t_R$ by means of the following functional relations

$$Q_R^{ST}(t;t_C,\lambda,t_R) = Q_R^{ST}(\frac{t}{t_C};\lambda,\frac{t_R}{t_C}) \quad (69)$$

$$Q_R^{LT}(t;t_C,\lambda,t_R) = Q_R^{LT}(\frac{t}{t_C};\lambda,\frac{t_R}{t_C}) \quad (70)$$

In analogy with Eqs. 34, 35, and 36, we form the following squared-error relations

$$E_R^{ST}(t_C,\lambda,t_R,i_m) = \sum_{i=0}^{i_m}\left(Q_{R_i} - Q_R^{ST}(\frac{t_i}{t_C},\lambda,\frac{t_R}{t_C})\right)^2 \quad (71)$$

$$E_R^{LT}(t_C,\lambda,t_R,i_m) = \sum_{i=i_m}^{n-1}\left(Q_{R_i} - Q_R^{LT}(\frac{t_i}{t_C},\lambda,\frac{t_R}{t_C})\right)^2 \quad (72)$$

$$E_R(t_c,\lambda,t_R,i_m) = E_R^{ST}(t_c,\lambda,t_R,i_m) + E_R^{LT}(t_c,\lambda,t_R,i_m) \quad (73)$$

These are the expressions that will be used to obtain a best fit of the theoretical curves with the experimental data

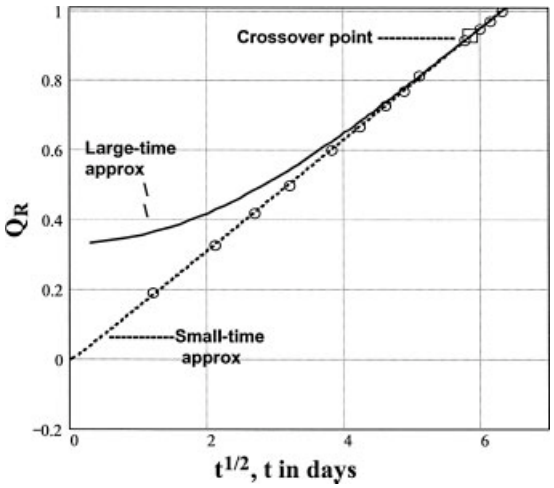


**Figure 7. Results of regression analysis showing correlation of Sachs[5] 40°C data with time-limited theory: $t_R$ = 39.9 days; $\lambda$ = 1.5625, $t_C$ = 159 days.**

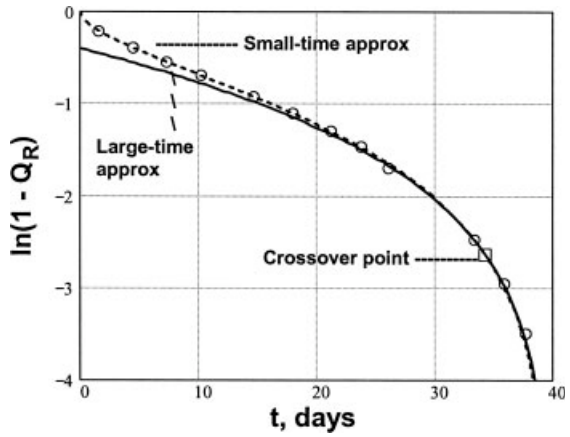


**Figure 8. Results of regression analysis for Sachs[5] 40°C data shown on semilog plot for time-limited formulation: $t_R$ = 39.9 days; $\lambda$ = 1.5625, $t_C$ = 159 days.**

by means of a formal regression analysis. The corresponding expressions associated with the time-limited semilog plots, analogous to Eqs. 37–39, are not listed here because they are not used, in favor of Eqs. 71–73.

## Applications to Gas Diffusion Tests

The input data consists from the fluid data and pressure decay data. The fluid data includes the solute type, such as $CH_4$ or $CO_2$, the solvent type, such as water or oil, the heights of liquid and gas columns in the PVT cell $L$ and $H$, and the temperature of the system $T$, assumed to be maintained constant in this study. The pressure decay data are the pressure values measured at various times, i.e., $p_i$ vs. $t_i$ for $i$ = 1, 2, ……$n$-data points, obtained during the isothermal pressure decay tests. The data used here for illustration purposes were extracted from various publications by first scanning and then digitizing the reported data in the form of plots. Hence, this process might have introduced some inherent errors in the data obtained this way in addition to the errors involved in the measurement of the experimental data. The reference value of the gas pressure was taken as the last value measured in the pressure decay tests. The real gas deviation factor $Z$ was predicted according to Peress.[26]

### *Analysis of the data of Sachs*

This modeling approach neglected the effect of swelling considering that the gas-liquid solution is dilute, and, therefore, behaves as an ideal solution during the time-limited tests. In fact, based on the experimental data provided by Sachs[5] for the $CH_4$-water system, the percentages of the initial mass of gas dissolved over the periods of the complete tests are only 0.74% for the tests ran at 25°C and 2.6% for 40°C. These findings justify the validity of the assumptions made for the development and applicability of this model.

A set of 13 discrete data points, representing the time-limited ($t_R$ = 39.9 days) description of Sachs[5] 40°C data, is plotted vs. $\sqrt{t}$ in Figure 7, and as a semilog plot in Figure 8. The theoretical curves were calculated using the values $\lambda$ = 1.5625 and $t_C$ = 159 days obtained from a regression analysis using Eq. 73. The result of determining the least value of $E_R$ is shown in Figure 9, where $E_R$ is plotted as a function of $t_C$ for three separate values of $\lambda$, with the middle value providing the smallest value of $E_R$, all at a fixed value of $i_m$, in this case for $i_m$ = 9. The regression analysis involves making several figures akin to Figure 9, but for different values of $i_m$. On one of these graphs, the curve for the middle value of $\lambda$ will contain the smallest value of $E_R$, located at the lowest point on the curve, out of all the similar values of $E_R$ pertaining to all the other curves for various fixed values of $\lambda$, and pertaining to the other graphs having fixed values of $i_m$. This pertinent graph is shown here as Figure 9, and the circled dot on the middle curve for $\lambda$ provides the values of $\lambda$ and $t_C$ together with the value of $i_m$ = 9 that renders $E_R$ a minimum. A summary of the pertinent results of the regression analysis, plus the values of the pertinent parameters

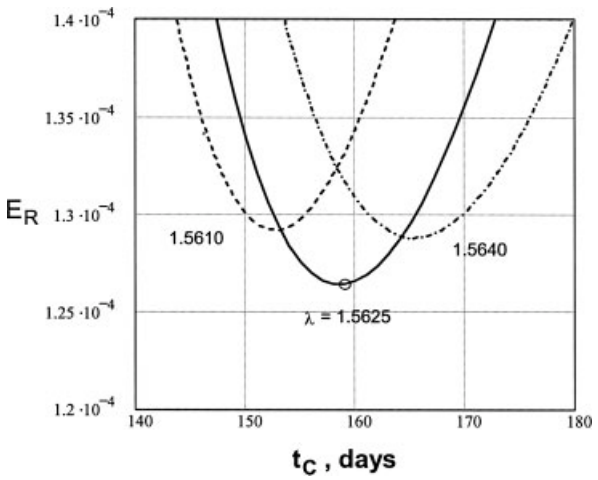


**Figure 9. Results of regression analysis showing minimum squared error for Sachs[5] 40°C data.**

**Table 1. Parameters of the Gas Diffusion Tests**

| Parameters | Sachs[5] | Sachs[5] | Sheikha et al.[10] Method #1 | Sheikha et al.[10] Method #2 |
|---|---|---|---|---|
| Solute | $CH_4$ | $CH_4$ | $CO_2$ | $CO_2$ |
| Solvent | Water | Water | Bitumen | Bitumen |
| Solvent height $L$, m | 0.048 | 0.189* | 0.0101 | 0.0101 |
| Gas height $H$, m | Not given | Not given | 0.0199 | 0.0199 |
| Initial solute concentration in solvent $c_o$, kg/m$^3$ | 0.0 | 0.0 | 0.0 | 0.0 |
| Temperature $T$, °C | 25 | 40 | 75 | 75 |
| Initial pressure $p_o$, MPa | 8.16 | 7.98 | 4.00 | 4.00 (3.95)** |
| Eigenvalue $\lambda$, dimensionless | $\pi/2$ | 1.5625 | $\pi/2$ | 1.5192 |
| Characteristic time $t_C$ | 18.97 days | 159 days | 56.3 hours | 57.9 hours |
| End-point reference time $t_R$ | 5.04 days | 39.9 days | 41.324 hours | 41.324 hours |
| Reported diffusion coefficient for the solute-solvent system $D$, m$^2$/s | $1.4 \times 10^{-9}$ | $2.6 \times 10^{-9}$ | $5.08 \times 10^{-10}$ | $4.64 \times 10^{-10}$ |
| Present diffusion coefficient for the solute-solvent system $D$, m$^2$/s | $1.406 \times 10^{-9}$ | $2.6 \times 10^{-9}$ | $5.033 \times 10^{-10}$ | $4.894 \times 10^{-10}$ |
| Present interface mass transfer coefficient $k$, m/s | Infinity | $2.59 \times 10^{-6}$ | Infinity | $1.426 \times 10^{-6}$ |
| Mass-transfer Biot number $k_D$, dimensionless | Infinity | 188.3 | Infinity | 29.42 |
| Reported equilibrium pressure $p^*$, MPa | 8.10*** | 7.77*** | 3.24 | 3.24 |
| Present equilibrium pressure $p^*$, MPa | 8.05 | 7.79 | 3.13 | 3.13 |
| Present equilibrium solubility $c^*$, kg/m$^3$ | Insufficient data | Insufficient data | 34.30 | 33.37 |
| Coefficient of regression $R^2$ | 0.999938 | 0.993995 | 0.999142 | 0.999927 |

*Value not given and therefore estimated to match the diffusion coefficient value reported by Sachs.[5]
**Present results only.
***Approximated by extrapolation.

associated with the experimental setup; along with values of the diffusion and film mass-transfer coefficients gleaned from them, is given in Table 1.

The corresponding results for Sachs[5] 25°C data are shown in Figures 10, 11, and 12. These results are based on the time-limited formulation ($t_R$ = 5.04 days) of the set of 14 discrete data points, with the theoretical curves fitted to the data using the values $\lambda=\pi/2$, $t_C$ = 18.97 days, and $i_m$ = 10 stemming from a regression analysis using Eq. 73. For this case, the early-time data in Figure 10 are fitted by a straight line passing through the origin ($\lambda = \pi/2$), which, as it turns out, provides a good fit for nearly all the data. This is verified also by Figure 11. The fact that $\lambda = \pi/2$ is a limiting value for $\lambda$ is demonstrated also by the results of the regression analysis shown in Figure 12. The best estimate parameter values yielding the best fit of the experimental data are reported in Table 1.

### *Analysis of the data of Sheikha et al.*

The next two sets of figures (Figures 13–15 and 16–18) analyze the data used by Sheikha et al.[10] for the $CO_2$ - bitumen system at 75°C. Twenty-two data points were used, with $t_R$ = 41.32 h. The first case (Figures 13, 14, and 15) is for the initial pressure taken to be $p_o$ = 4.00 MPa. The theoreti-

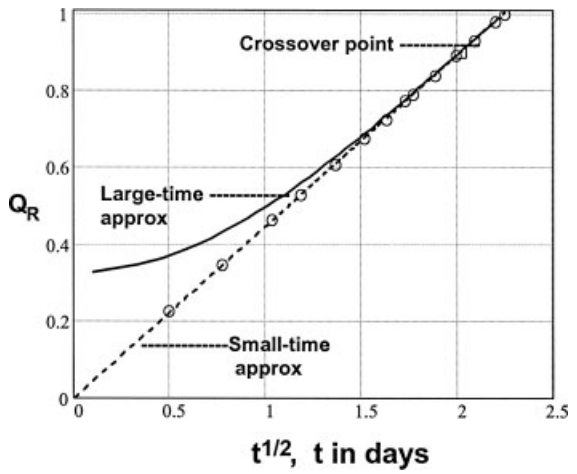


**Figure 10. Results of regression analysis showing correlation of Sachs[5] 25°C data with time-limited theory: $t_R$ = 5.04 days; $\lambda = \pi/2$, $t_C$ = 18.97 days.**

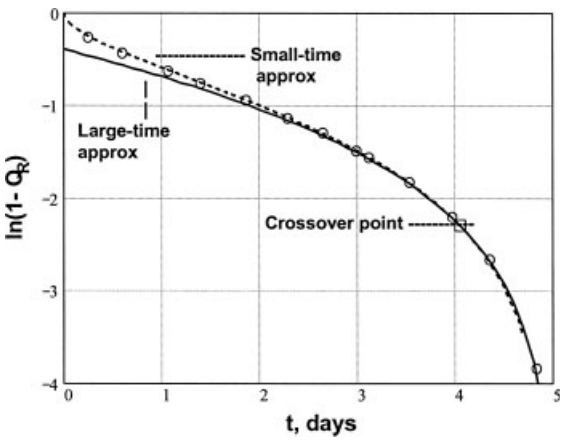


**Figure 11. Results of regression analysis for Sachs[5] 25°C data shown on semilog plot for time-limited formulation: $t_R$ = 5.04 days; $\lambda = \pi/2$, $t_C$ = 18.27 days.**

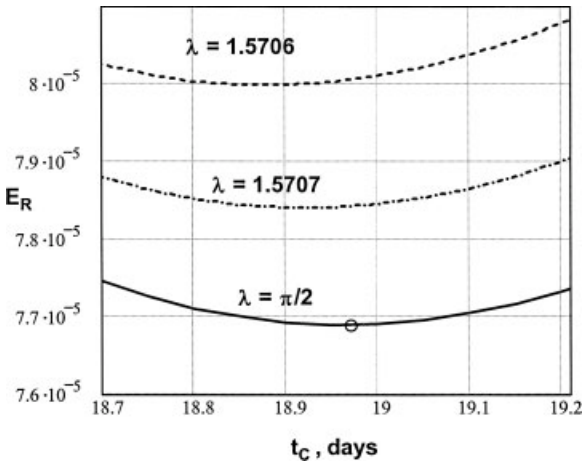


**Figure 12. Results of regression analysis showing minimum squared error for Sachs[5] 25°C data.**

cal curves were fitted to the data using the values $\lambda = \pi/2$, $t_C = 56.3$ h, and $i_m = 10$, resulting from a regression analysis using Eq. 73. The corresponding value of the diffusion coefficient is $D = 5.033 \times 10^{-10}$ m$^2$/s, which is slightly smaller than the value $D = 5.08 \times 10^{-10}$ m$^2$/s reported by Sheikha et al.[10] obtained by their graphical method #1.

It was observed during the course of this analysis that the early-time data in Figure 13 lie above the limiting ($\lambda = \pi/2$) straight-line small-time approximation, which is inconsistent with the underlying theory. After perusing the original pressure-decay curve $p = p(t)$, it was concluded that the data could be faired back more smoothly to an initial pressure $p_o = 3.95$ MPa, which was lower than the reported value $p_o = 4.00$ MPa, used in the calculations. Thus, a new set of calculations was made, shown in Figures 16, 17, and 18, with a new initial pressure taken to be $p_o = 3.95$ MPa. A new regression analysis yielded the values $\lambda = 1.5192$, $t_C = 57.9$ h, and $i_m = 10$. The diffusion coefficient and interface mass-

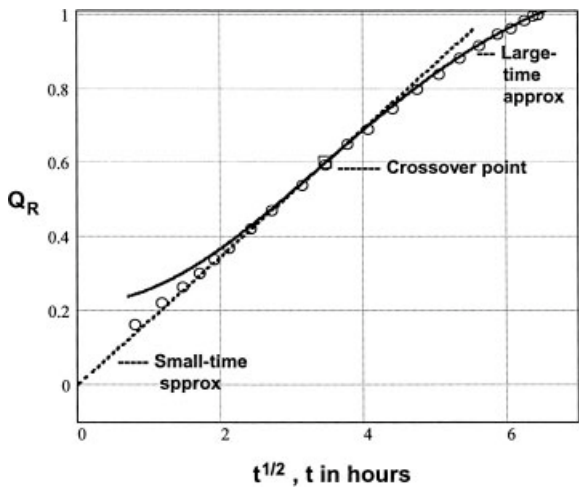


**Figure 13. Results of regression analysis showing correlation of Sheikha et al.[10] data with time-limited formulation for $p_o = 4.00$ Mpa, $t_R = 41.32$ hours; $\lambda = \pi/2$, $t_C = 56.3$ hours.**

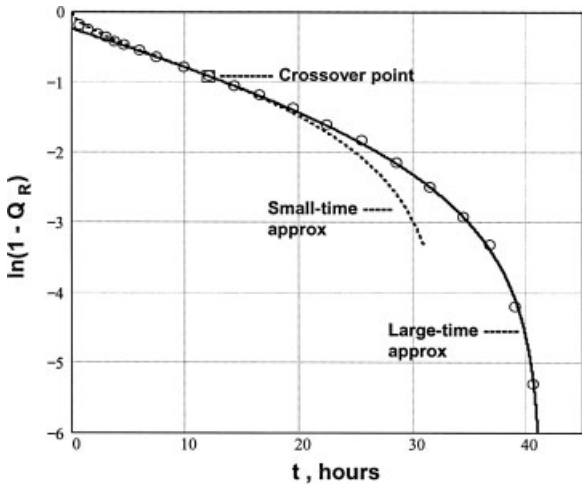


**Figure 14. Results of regression analysis showing correlation of Sheikha et al.[10] data on semilog plot with time-limited formulation for $p_o = 4.00$ MPa, $t_R = 41.32$ hours; $\lambda = \pi/2$, $t_C = 56.3$ hours.**

transfer coefficient were found to be $D = 4.894 \times 10^{-10}$ m$^2$/s and $k = 1.426 \times 10^{-6}$ m/s. In this case, a 1.25% decrease in initial pressure led to a 2.17% decrease in the diffusion coefficient. Notice also in Figure 16 the pronounced curvature in the curve for the small-time approximation, as well as the good correlation with the data, compared with the corresponding straight line in Figure 13. This leads also to the finite value of $k_D = 29.42$ for the new analysis.

The figure of merit for the overall quality of the fitted data is the coefficient of regression $R^2$ (Chapra and Canale[25]). It is given in Table 1 for each of the cases considered (the closer to unity the better).The smaller the value of $E_R$ shown in Figures 9, 12, 15, and 18 is also indicative of the quality of fit. The values of $R^2$ shown in Table 1 for the four different cases, being so close to unity, indicates that the quality of the curve fits is very good for each. If one compares the results of this analysis depicted by Figures 13, 14, and 15 for

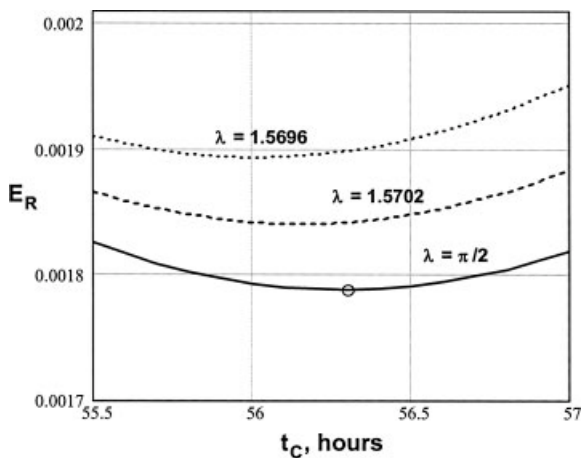


**Figure 15. Results of regression analysis showing minimum squared error for Sheikha et al.[10] data for $p_o = 4.00$ MPa.**

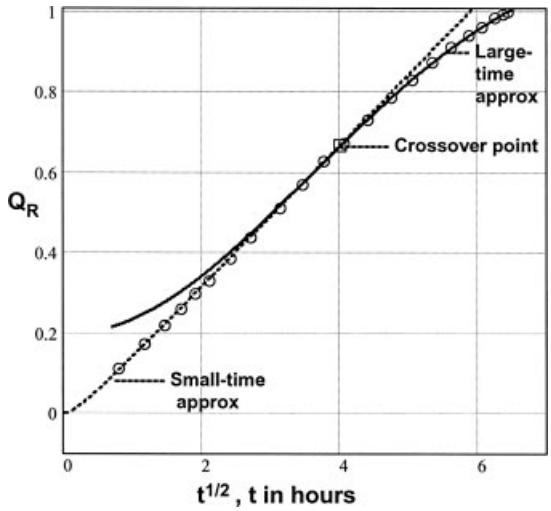


**Figure 16. Results of regression analysis showing correlation of Sheikha et al.[10] data with time-limited formulation for $p_o$ = 3.95 MPa, $t_R$ = 41.32 hours; $\lambda$ = 1.5192, and $t_C$ = 57.9 hours.**

the initial pressure $p_o$ = 4.00 MPa, with the results depicted by Figures 16, 17, and 18 for $p_o$ = 3.95 MPa, all other given data being equal, one finds that the fitted curve for the $p_o$ = 3.95 MPa case is the superior of the two as adjudged by the relative values of $R^2$, as well as the lower value of $E_R$. Consequently, the values of the diffusion coefficient $D$, and the interface mass-transfer coefficient $k$ for this case, are regarded as the best-estimate values.

This time-limited data-reduction method allows for the equilibrium pressure $p^*$ to be calculated. This is done by means of Eq. 55. The equilibrium solubility $c^*$ is calculated by means of Eq. 15. The results are shown in Table 1 for the four cases considered, along with reported values.

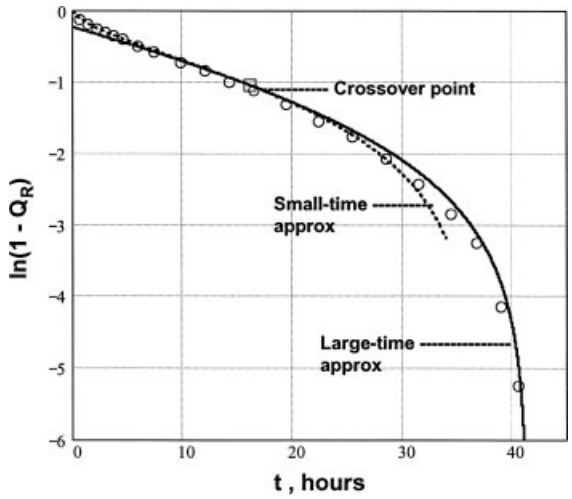


**Figure 17. Results of regression analysis showing correlation of Sheikha et al.[10] data on semilog plot with time limited formulation for $p_o$ = 3.95 MPa.**

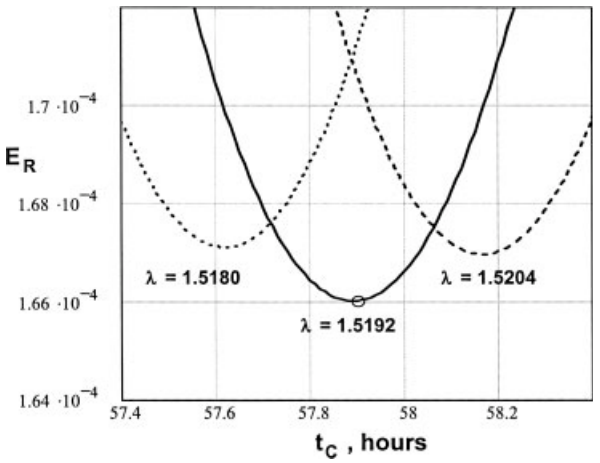


**Figure 18. Results of regression analysis showing minimum squared error for Sheikha et al.[10] data for $p_o$ = 3.95 MPa.**

## Conclusions

This methodology was proven practical, yielding unique and accurate values simultaneously for the diffusion and interface-mass transfer coefficients, and the equilibrium pressure and gas solubility. In contrast, the previous approaches can only determine the diffusion coefficient. The parameters calculated by previous methods may involve error when the time required for reaching equilibrium between the gas and liquid phases is relatively long, like several months, because of appreciable liquid swelling by increased amount of gas dissolution and possible gas leak from high-pressure PVT-cells. Being able to process time-limited data, this method may conveniently circumvent such errors.

## Notation

$a$ = $y$-axis intercept of straight line
$A$ = cross-sectional area of the test tank, $L^2$
$b$ = slope of straight line
$c$ = gas mass concentration of the gas-liquid solution, $M/L^3$
$c^*$ = equilibrium solubility, $M/L^3$
$C$ = gas molar concentration in the liquid, $Mol/L^3$
$D$ = gas diffusivity in the liquid, $L^2/T$
$D_o$ = diffusion coefficient for a nonswelling liquid, $L^2/T$
$D_s$ = diffusion coefficient for a swelling liquid, $L^2/T$
$E$ = total squared error
$H$ = height of the gas column, L
$i_m$ = point that separates the short-time data from the long-time data
$i_o$ = first data point to be included in the analysis
$J$ = gas mass flux, $M/L^2$-T
$k$ = interface mass-transfer coefficient, L/T
$K_H$ = Henry's constant, $L^2/T^2$
$L$ = height of the liquid column, L
$L_o$ = liquid height for a nonswelling liquid, L
$L_s$ = liquid height for a swelling liquid, L
$m$ = instantaneous amount of the gas, M
$m_o$ = initial amount of the gas, M
$M$ = molecular weight of gas, M/mol
$p$ = pressure, $M/L\text{-}T^2$
$p^*$ = equilibrium pressure, $M/L\text{-}T^2$
$Q_D$ = dimensionless cumulative gas mass dissolved in the liquid phase, $M/L^2$

$R^2$ = coefficient of regression, dimensionless
$\Re$ = universal gas constant, $ML^2/mol\text{-}\theta\text{-}T^2$
$x$ = distance measured from the gas-liquid interface into the liquid phase, L
$t$ = time, T
$T$ = temperature, $\theta$
$V$ = volume, $L^3$
$Z$ = real-gas deviation factor, dimensionless
$z = k_D\sqrt{t_D}$ = variable in Eq.26

### Greek letters

$\lambda$ = root of Eq. 20, dimensionless

### Subscripts

$C$ = characteristic value
$CO$ = crossover point
$D$ = dimensionless
$g$ = gas
$LT$ = long-time
$ST$ = short-time
$o$ = initial or reference state
$R$ = reference measurement value

### Superscripts

$LT$ = long-time
$ST$ = short-time
$^*$ = equilibrium state

## Literature Cited


1. Hill ES, Lacey WN. Rate of solution of propane in quiescent liquid hydrocarbons. *Ind Eng Chem*. 1934;12:1327–1331.
2. O'Bryan PL, Bourgoyne Jr.AT, Monger TQ, Kopcso DP. An experimental study of gas solubility in oil-based drilling fluids. *SPE Drilling Eng*. 1988;3:133–142.
3. O'Bryan PL, Bourgoyne Jr.AT. Swelling of oil-based drilling fluids resulting from dissolved gas. *SPE Drilling Eng*. 1990;5(2):149–155.
4. Riazi MR. A new method for experimental measurement of diffusion coefficients in reservoir fluids. *J. Petroleum Sci Eng*. 1996;14:235–250.
5. Sachs W. The diffusion of methane in water at reservoir conditions, A first attempt. *Erdol Erdgas Kohle*. 1997;113:177–179.
6. Sachs W. The diffusional transport of methane in liquid water: method and result of experimental investigation at elevated pressure. *J Petroleum Sci Eng*. 1998;21:153–164.
7. Zhang YP, Hyndman CL, Maini BB. Measurement of gas diffusivity in heavy oils. *J Petroleum Sci Eng*. 2000;25:37–47.
8. Upreti SR, Mehrotra AK. Diffusivity of $CO_2$, $CH_4$, $C_2H_6$, and $N_2$ in athabasca bitumen. *Can J Chem Eng*. 2002;80:116–125.
9. Tharanivasan AK, Yang C, Gu Y. Comparison of three different interface mass transfer models used in the experimental measurement of solvent diffusivity in heavy oil. *J Petroleum Sci Eng*. 2004;44:269–282.
10. Sheikha H, Pooladi-Darvish M, Mehrotra AK. Development of graphical methods for estimating the diffusivity coefficient of gases in bitumen from pressure-decay data. *Energy Fuels*. 2005;19:2041–2049.
11. Sheikha H, Mehrotra AK, Pooladi-Darvish M. An inverse solution methodology for estimating the diffusion coefficient of gases in Athabasca bitumen from pressure-decay data. *J Petroleum Sci Eng*. 2006;53:189–202.
12. Sheikha H, Pooladi-Darvish M, Mehrotra AK. The importance of graphical methods in estimation of the diffusion coefficient of gases in bitumens and heavy oil, Paper SPE 101057, presented at the SPE Annual Technical Conference and Exhibition; 24-27 September, 2006; San Antonio, TX.
13. Civan F, Rasmussen ML. Accurate Measurement of gas diffusivity in oil and brine under reservoir conditions. *Paper SPE 67319, SPE Mid-Continent Operations Symposium, 2001*. Oklahoma City, OK; March 2001.
14. Civan F, Rasmussen ML. Improved measurement of gas diffusivity for miscible gas flooding under nonequilibrium vs. equilibrium conditions. *Paper SPE 75135, SPE/DOE Thirteenth Symposium on Improved Oil Recovery*. Tulsa, OK; 13-17 April 2002.
15. Civan F, Rasmussen ML. Analysis and interpretation of gas diffusion in quiescent reservoir, drilling, and completion fluids: Equilibrium vs. non-equilibrium models, Paper SPE 84072, SPE Annual Technical Conference and Exhibition; 5 - 8 October, 2003; Denver, CO.
16. Civan F, Rasmussen ML. Determination of gas diffusion and interface-mass transfer coefficients for quiescent reservoir liquids. *SPE J*. 2006;11:71–79.
17. Renner TA. Measurement and correlation of diffusion coefficients for $CO_2$ and rich-gas applications. *SPE Reservoir Eng*. 1988;3:517–523.
18. Jamialahmadi M, Emadi M, Müller-Steinhagen H. Diffusion coefficients of methane in liquid hydrocarbons at high pressure and temperature. *J Petroleum Sci Eng*. 2006;53:47–60.
19. Wen Y, Bryan J, Kantzas A. Estimation of diffusion coefficients in bitumen solvent mixtures as derived from low field NMR spectra. *J Can Petroleum Technol*. 2005;44:29–35.
20. Wen YW, Kantzas A. Monitoring bitumen-solvent interactions with low-field nuclear magnetic resonance and X-ray computer-assisted tomography. *Energy Fuels*. 2005;19:1319–1326.
21. Morgan D, Ferguson L, Scovazzo P. Diffusivities of gases in room-temperature ionic liquids: Data and correlations obtained using a lag-time technique. *Ind Eng Chem Res*. 2005;44:4815–4823.
22. Yang CD, Gu YA. New experimental method for measuring gas diffusivity in heavy oil by the dynamic pendant drop volume analysis (DPDVA). *Ind Eng Chem Rese*. 2005;44:4474–4483.
23. Walas SM. *Modeling with Differential Equations in Chemical Engineering*. Boston: Butterworth-Heinemann Series in Chemical Engineering; 1991.
24. Crank J. *The Mathematics of Diffusion*. London: Oxford University Press; 1956.
25. Chapra SC, Canale RP. *Numerical Methods for Engineers*. 2nd ed. New York, NY: McGraw-Hill; 1998.
26. Peress J. Working with non-ideal gases. *Chem Eng Progr*. 2003;99:39–41.
27. Shiflett MB, Yokozeki A. Solubility and diffusivity of hydrofluorocarbons in room-temperature ionic liquids. *AIChE J*. 2005;52:1205 – 1219.
28. Churchill RV. *Modern Operational Mathematics in Engineering*. 3rd ed. New York, NY: McGraw-Hill; 1972.


## Appendix A: Gas-Liquid Interface Boundary Condition and Liquid Swelling

Sheikha et al.[10–12] and Jamialahmadi et al.[18] considered a thermodynamic equilibrium at the interface between the gas and liquid phases. Applying the film theory, the equilibrium dissolved gas concentration $c$ in the liquid phase near the interface corresponding to the gas pressure $p$ in the gas phase was considered as the boundary condition. Sheikha et al.[10–12] applied Henry's law, given by

$$p = K_H c \tag{A1}$$

where $K_H$ is Henry's constant. The applicability of Eq. A1 is limited to dilute solutions. Jamialahmadi et al.[18] measured their experimental data, while maintaining the applied gas pressure constant above the liquid phase. Hence, their interface boundary condition dictates that the dissolved gas concentration near the interface remains constant; i.e. $c$ = ct. In contrast, Sheikha et al.[10–12] conducted their experiments by applying the pressure decay method. Hence, the applied gas pressure varied with time. Therefore, Eq. A1 contains two

variables and a second equation is needed. The latter has been obtained by incorporating the Fick's law of diffusion for transfer of the gas component from the gas phase to the liquid phase at the interface into the mass balance of the gas phase as

$$-\frac{dm_g}{dt} = j = -DA\left.\frac{\partial c}{\partial x}\right|_{x=0} \tag{A2}$$

Thus, combining Eqs. A1, A2, and 11 leads to

$$\mathrm{DA}\left.\frac{\partial c}{\partial x}\right|_{x=0} = \frac{\mathrm{MK}_H c|_{x=0}}{\mathrm{Z}\Re\mathrm{T}}\frac{dV}{dt} + \frac{\mathrm{VMK}_H}{\Re\mathrm{T}}\left[\frac{1}{Z} - \frac{K_H c|_{x=0}}{Z^2}\left(\frac{\partial Z}{\partial p}\right)_T\right]\frac{dc|_{x=0}}{dt} \tag{A3}$$

Sheikha et al.[10–12] neglected the variation of the volume of the gas phase by swelling of the liquid phase owing to gas dissolution, and the term involving the partial derivative of the real gas deviation factor with respect to pressure. The nonequilibrium boundary condition (Eq. 6) used in this study conveniently alleviates these problems.

The measurements by Yang and Gu[22] indicated less than 11% increase in the liquid volumes measured at 4.0 MPa during the dissolution of carbon dioxide in heavy oil. Jamialahmadi et al.[18] observed a rapid and large increase in the liquid volume by swelling at elevated pressures. For example, the height of the liquid column increased by 22% at 24 MPa (3,500 psia) during dissolution of methane in dodecane in a very long time period of 90 h. In contrast, the fluid height increased only by 3.7% at 6.9 MPa (1,000 psia) during the same time period. The fluid level increase during the experiments conducted by Sachs[5] around 8.1 MPa (1,175 psia) is expected to be less than 4%. Shiflett and Yokozeki[27] estimated the effect of the systematic errors owing to the variation of the fluid height by gas absorption, and other factors to be less than a factor of two in the determined value of the diffusion coefficient. Because the diffusion coefficient relates to the diffusion length-squared proportionally, the affect of the variations of the liquid level by swelling may be roughly estimated as

$$\frac{D_s - D_o}{D_o} = \left(\frac{L_s - L_o}{L_o} + 1.0\right)^2 - 1.0 \tag{A4}$$

where $D_o$ and $L_o$ denote the diffusion coefficient and the liquid height for a nonswelling liquid, and $D_s$ and $L_s$ denote the respective quantities for a swelling liquid. Thus, for example, if the liquid height rises by 10% owing to swelling, then the diffusion coefficient should increase by 21%.

## Appendix B: Estimation of Error

The error in the long-time approximation that is incurred by retaining only the leading term in the infinite series (Eq. 19), can be estimated by comparison with the result obtained by keeping the first two terms of the series. The decimal error can then be expressed as

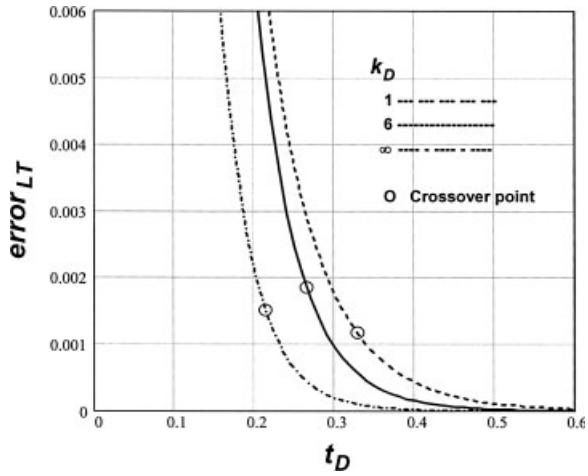


**Figure B1. Error incurred in long-time approximation by keeping only leading term of infinite series as a function of $t_d$ for $k_d$ = 1, 6, and ∞; the small circles indicate the location of the crossover points.**

$$error_{LT}(t_D, k_D) = \frac{Q_1(\lambda_2)\exp(-\lambda_2^2 t_D)}{1 - Q_1(\lambda_1)\exp(-\lambda_1^2 t_D)} \tag{B1}$$

where $\lambda_1$ and $\lambda_2$ are valid in the respective ranges of $0 \le \lambda_1 \le \pi/2$ and $\pi \le \lambda_2 \le 3\pi/2$ as $k_D$ varies from zero to infinity according to Eq. 20. Figure B1 shows the decimal error that is incurred by using only the first term of the series, plotted as a function of $t_D$ for values of $k_D$ = 1, 6, and ∞. The circles on these curves indicate the location of the crossover points (the point $t_D = t_{Dco}$ where $Q_D^{LT} = Q_D^{ST}$ for a given value of $\lambda_1 = \lambda_1(k_D)$). Data for the crossover points are shown in Figure 2. The long-time approximation for $Q_D$ is valid strictly when $t_D > t_{Dco}$. The error for $Q_D^{LT}$ given by Eq. 21 is largest at $t_D = t_{Dco}$ and dies out rapidly as $t_D$ increases. When $k_D$ = 6.015, for instance, then $t_{Dco}$ = 0.2645, and the decimal error is, $\mathrm{Error_{LT}}$ = 0.001863, or 0.1863%. This means that $Q_D^{LT}$ = 0.4430 is too large by 0.1863%. Thus, the corrected value should be 0.4422. This difference is regarded as negligible. Although this example holds for the maximum error for $k_D$ = 6.015, further analysis would show that the maximum values for arbitrary values of $k_D$ are less than or approximately equal to the example value. On these grounds, therefore, Eq. 21 is justified as an accurate long-time approximation, having a maximum error of less than 0.2% when $t_D > t_{Dco}$.

The error that is incurred in the short-time approximation by the use of only the semi-infinite solution, Eq. 24, can be estimated as follows. The first-order terms of the short-time expansion for the Laplace transform of the mass-accumulation function are, for the finite-volume case

$$\begin{aligned}\overline{Q}_D^{ST}(s) &= \frac{k_D}{s}\frac{1 - e^{-2\sqrt{s}}}{s + k_D\sqrt{s}} + (\text{higher} - \text{order terms}) \\ &= \left(\frac{1}{s\sqrt{s}} - \frac{1}{s(\sqrt{s} + k_D)}\right)(1 - e^{-2\sqrt{s}}) + (h.o.t.)\end{aligned} \tag{B2}$$

where $s$ is the Laplace-transform variable. Because small times correspond to large values of the transform variable $s$, the exponential factor $e^{-2\sqrt{s}}$ is a measure of smallness in the expansion process. It appears in the first-order approximation as a result of enforcing the zero mass-flux boundary condition at $x_D = 1$. Consequently, in the transform of the first-order terms shown in Eq. B2, the first term in the numerator holds for the semi-infinite case, and the exponential second term describes the correction that accounts for the finite-volume case. The inversions of the first-order terms are readily accomplished by means of standard Laplace-transform tables (Churchill[28]), and we get

$$Q_D^{ST}(t_D) = (Q_D^{ST}(t_D))_\infty - (Q_D^{ST}(t_D))_{\Delta V} + (h.o.t.) \tag{B3}$$

where

$$(Q_D^{ST}(t_D))_\infty \equiv \frac{1}{k_D}\left[\exp(k_D^2 t_D)\mathrm{erfc}(k_D\sqrt{t_D}) - 1 + 2k_D\sqrt{\frac{t_D}{\pi}}\right] \tag{B4}$$

$$(Q_D^{ST}(t_D))_{\Delta V} \equiv \frac{1}{k_D}\left[2k_D\sqrt{\frac{t_D}{\pi}}\exp\left(-\frac{1}{t_D}\right) - (2k_D+1)erfc\left(\frac{1}{\sqrt{t_D}}\right) + e^{2k_D+k_D^2 t_D}erfc\left(k_D\sqrt{t_D}+\frac{1}{\sqrt{t_D}}\right)\right] \tag{B5}$$

In the first-order short-time approximation, the decimal error incurred by neglecting the finite-volume effects is

$$error_{ST}(t_D, k_D) = \frac{(Q_D^{ST}(t_D))_{\Delta V}}{(Q_D^{ST}(t_D))_\infty} \tag{B6}$$

The decimal error incurred is plotted in Figure B2 as a function of $t_D$ for $k_D = 1$, 6, and $\infty$; the small circles indicate the location of the crossover points. The short-time approximation is valid strictly in the range $0 \le t_D \le t_{Dco}$. Thus, for a given $k_D$, the maximum decimal error occurs at $t_{Dco}$. For $k_D = \infty$ and $k_D = 6$, the maximum decimal errors are 0.000762, or 0.0762%, and 0.001652, or 0.1657%, respectively. For the range of $k_D$ shown in Figure B2, the curve for $k_D = 1$ has the largest decimal error, which is 0.003109, or 0.3109%. These errors are so small that they hardly make a difference in the drawn curves for $Q_D$ vs. $t_D$, These are the grounds for which Eq. 24 has been deemed to accurately describe the short-time behavior of $Q_D$ in the range $0 \le t_D \le t_{Dco}$.

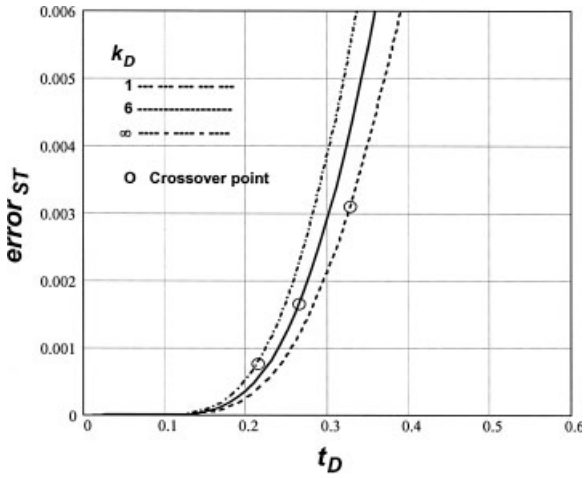


**Figure B2. Error incurred in short-time approximation by neglecting effects of finite volume as a function of $t_d$ for $k_d$ = 1, 6, and ∞; the small circles indicate the location of the crossover points.**

*Manuscript received Feb. 4, 2008, revision received Apr. 25, 2008, and final revision received Aug. 21, 2008.*